Catalysis Today 176 (2011) 242–249

Contents lists available at ScienceDirect

Catalysis Today

journal homepage: www.elsevier.com/locate/cattod

Palladium catalysts supported on sulfated ceria–zirconia for the selective catalytic reduction of NO_x by methane: Catalytic performances and nature of active Pd species

B. Azambre[a,*], L. Zenboury[a], P. Da Costa[b], S. Capela[c], S. Carpentier[c], A. Westermann[a]

[a] Laboratoire de Chimie et Methodologies pour l'Environnement (LCME), Institut Jean-Barriol, Université Paul Verlaine – Metz, IUT Chimie – Rue Victor Demange, 57500 Saint Avold, France
[b] Institut Jean Le Rond D'Alembert, Université Pierre et Marie Curie Paris 6, CNRS UMR 7190 – 2, place de la gare de ceinture, 78210 Saint Cyr l'Ecole, France
[c] Centre de Recherche et d'Innovation en Gaz et Energies Nouvelles (CRIGEN) de GDF SUEZ, 361 Avenue du Président Wilson, 93211 Saint Denis – La Plaine Cedex, France

ARTICLE INFO

Article history:
Received 22 September 2010
Received in revised form 9 December 2010
Accepted 9 December 2010
Available online 13 January 2011

Keywords:
NO_x
$Ce_xZr_{1-x}O_2$
CH_4-SCR
Sulfates
NO_2
CO adsorption
Palladium

ABSTRACT

Novel Pd sulfated ceria–zirconia catalysts for the SCR of NO_x by methane were prepared by impregnation of a $PdCl_2$ precursor dissolved in ammonia solution on a sulfated $Ce_{0.21}Zr_{0.79}O_2$ support, itself obtained by direct sulfation of a ceria–zirconia nanopowder in 0.5 M H_2SO_4. Best CH_4-SCR performances under the conditions 150 ppm NO; 1500 ppm CH_4; 7 vol.% O_2 were achieved using Pd loadings in the range 0.24–0.53 wt.% with 30–35% NO conversion to N_2 around 350–400 °C. By contrast, the formation of a PdO_x phase at superior Pd loadings was found detrimental for the SCR activity because it promotes also the non-selective methane oxidation. Increasing CH_4 concentrations or adding H_2O to the feed have opposite trends on $DeNO_x$, activity, the latter being detrimental at low-medium temperatures due to inhibiting effects on adsorption. As evidenced by DRIFTS of CO and pyridine adsorption, UV–Vis, HRTEM–EDX and XRD, the nature of the Pd species active in SCR could be $[Pd(O)–H]^{x+}$ isolated species and/or small $[(PdO)_n–H]^{x+}$ clusters possessing a high Lewis acidity and a low reducibility.

1. Introduction

The selective catalytic reduction (SCR) of NO_x with methane is an attractive approach to pollution control due to the hydrocarbon availability through natural gas infrastructures. This after-treatment technology would be particularly applicable to stationary sources such as natural gas engines and small-scale gas boilers, in which unburned methane remains as a component in the exhaust. However, these engines typically operate under lean conditions in order to improve their efficiency. This presents a challenge to the SCR of NO_x, as hydrocarbon (HC) combustion with O_2 tends to deplete the reducing agent [1,2].

From the literature data, active CH_4-SCR catalysts can be separated within two broad categories. The first one includes Pd, Co, In, Mn, Ga, Ag and Fe ion-exchanged cations, used alone or in combination, on acidic zeolithes having the ZSM-5, MOR and FER structures [2–9]. Some of these catalysts, namely those which include Pd or Co, are capable to reach very high $DeNO_x$ activities around 450–550 °C under dry conditions [4,5]. However, most of them also deactivate in the presence of wet exhaust streams (such as those from combustion of fossil fuels) due to the deterioration of the zeolithic metastable structures or even the washout of supported cations from their ideal positions [4,5]. The second category is represented by the same active phases, but supported on metal oxides whose acid properties were generally increased prior to impregnation by the introduction of oxoanions, namely of the sulfate type, using different methods [10–13]. The most successful preparations of Pd, Co, Mn and Pd–Co catalysts supported on sulfated zirconia were found to have $DeNO_x$ activities rather comparable to those of the best zeolithic catalysts in addition to improved hydrothermal and thermal stabilities and resistance to SO_2 [10].

The link between these two categories is the stabilization of highly dispersed cationic species at low metal loadings, which is promoted by the Brönsted acidity of the support [1,10]. For Pd supported catalysts, it was claimed that CH_4-SCR active palladium species could have either the Pd^{2+}, $[Pd–O–Pd]^{2+}$, $H^+(PdO)H^+$ or the Pd^0 forms, among other possibilities [14 and references therein]. By contrast, it was proposed that PdO particles and/or mixed PdO_x/Pd^0 phases rather catalyze the non-selective hydrocarbon oxidation [15].

Surprisingly, ceria–zirconia supports have been only very scarcely used in HC-SCR reactions [16,17], presumably due to

* Corresponding author. Tel.: +33 387939106; fax: +33 387939101.
E-mail address: bazambre@univ-metz.fr (B. Azambre).

0920-5861/$ – see front matter © 2010 Elsevier B.V. All rights reserved.
doi:10.1016/j.cattod.2010.12.026

Table 1
elemental analyses and specific surface area of the different catalysts.

Catalysts	Label	S (wt.%)	Cl (wt.%)	S_{BET} ($m^2\ g^{-1}$)
$Ce_{0.21}Zr_{0.79}O_2$	CZ28	–	–	185
Sulfated $Ce_{0.21}Zr_{0.79}O_2$	SCZ28	1.70	–	179
$Pd/Ce_{0.21}Zr_{0.79}O_2$	Pd1.04%/CZ28	–	0.56	158
Sulfated $Pd/Ce_{0.21}Zr_{0.79}O_2$	Pd0.99%/SCZ28	1.63	1380 ppm	161
	Pd0.53%/SCZ28	1.85	<300 ppm	168
	Pd0.47%/SCZ28	2.09	500 ppm	144
	Pd0.24%/SCZ28	1.89	440 ppm	159

the well-known oxygen storage capacity (OSC) of ceria, which is thought to promote the detrimental combustion of the hydrocarbon rather than the SCR reaction [18]. However, ceria can also be sulfated [19], which allows in principle to tune both the acid–base and the OSC properties of sulfated ceria–zirconia catalysts. Recently, we have reported an extensive characterization of these materials [20]. In this study, the CH_4-SCR performances of sulfated ceria–zirconia catalysts loaded with different amounts of Pd are reported under a variety of reaction conditions and are compared with a conventional non-sulfated Pd catalyst. The nature of the SCR-active Pd species is also investigated using different analytical techniques.

2. Experimental

2.1. Preparation of Pd-supported catalysts

The ceria–zirconia (CZ) support ($Ce_{0.21}Zr_{0.79}O_2$, CZ28) was supplied by Rhodia (La Rochelle) and obtained from nitrate precursors. Sulfated ceria–zirconia (SCZ28) was obtained as follows: 5 g of the bare support was reacted with 75 mL of sulfuric acid (0.46 M) for 45 min, filtered, washed with diluted H_2SO_4 (0.05 M), dried at 70 °C under vacuum and finally calcined at 500 °C (2 h). Pd-supported catalysts with different loadings in Pd (between 0.24 and 5 wt.%) were prepared by incipient wetness impregnation of CZ28 or SCZ28 using appropriate amounts of a $PdCl_2$ precursor (purity 99%, Aldrich) dissolved in NH_3. After drying under vacuum at 70 °C, the catalysts were calcined under air at 500 °C during 2 h. A list of the catalysts prepared and their corresponding labels are given in Table 1.

2.2. Characterization of the catalysts

The specific surface area (BET method, N_2 adsorption at 77 K) of the different prepared catalysts and their Pd, S and Cl contents, as determined from elemental analyses, are given in Table 1. Powder X-ray diffraction (XRD) measurements were performed on a Siemens D-500 diffractometer using Cu Kα monochromatized radiation from 10 up to 80° (2θ). HRTEM/EDX analyses of some selected catalysts previously dispersed in ethanol and deposited onto a perforated carbon foil supported on a copper grid were carried out on a JEOL-JEM 2011 UHR microscope operating at 200 kV (0.194 nm resolution). Solid UV–Vis spectra were recorded in the 190–800 nm range on a Varian Cary 5E spectrometer equipped with an integration sphere coated with polytetrafluoroethylene (PTFE). The sulfated ceria–zirconia support was used as reference.

Diffuse reflectance spectra (DRIFTS) were recorded in the 4000–700 cm^{-1} range (resolution 4 cm^{-1}, 100 scans) on a Bio-Rad FTS 185 spectrometer equipped with a MCT detector, a "Graseby Specac" optical accessory and a Spectra-Tech environmental cell. IR acidity studies using pyridine adsorption were carried out at 60 °C into a static home-made adsorption cell, allowing the catalysts pre-treatment at 130 °C under dynamic vacuum. After 24 h, physisorbed pyridine was removed by purging the catalysts at 80 °C prior to their transfer to the FTIR spectrometer where DRIFTS spectra were recorded (using the corresponding unexposed catalyst pre-treated in the same conditions as reference). For the *in situ* DRIFTS experiments related to the examination of Pd supported catalysts by CO adsorption, the samples were first outgassed *in situ* under He up to 400 °C, cooled down to 30 °C and then CO (1000 ppm/He, 80 mL/min) was introduced at the same temperature in order to obtain time-resolved spectra corresponding to increasing CO exposures. Upon saturation by adsorbed CO, samples were purged under He and then heated up to 400 °C under He (ν = 10 °C/min) to study the thermostability of the different CO ad-species. In all this series of experiments, the background reference was the single-beam spectrum of the catalyst pre-treated at the same temperature before CO adsorption.

2.3. Catalytic tests

Prior to catalytic measurements, the calcined samples were pretreated *in situ* under Ar at 500 °C (10 °C/min) in a U-type quartz reactor itself placed inside a vertical furnace regulated with a Eurotherm controller. Temperature programmed surface reactions (TPSR) and isothermal tests were both carried out under the following conditions (unless otherwise stated): 150 ppm NO; 1500 ppm CH_4; 7 vol.% O_2; balance Ar; GHSV = 40,000 h^{-1}; $m_{catalyst}$ = 0.55 g. First, the temperature was ramped from 25 to 500 °C (ν = 10 °C/min) under the reactant mixture (TPSR mode) and then the SCR activity of the catalysts was measured under steady-state conditions back from 500 °C to 250 °C (dwells of 50 °C). The reactor outflow was monitored continuously using both an Eco Physics CLD 700 AL chemiluminescence NO_x analyzer (for NO, NO_2 and total NO_x), Ultramat 6 IR analyzers (N_2O, CO, CO_2) and a FID detector (FIDAMAT 5E) for the total concentration of hydrocarbons. A gas microchromatograph VARIAN CP 4900 (the capillary columns were PLOT 5A 10 m × 0.32 m ID and Paraplot Q 10 m × 0.15 m ID) was coupled to the experiment at the outlet of the reactor to monitor N_2.

The relative amounts of methane reacted with NO (SCR: $CH_4 + 2NO + O_2 \rightarrow N_2 + 2H_2O + CO_2$) and O_2 (combustion: $CH_4 + 2O_2 \rightarrow CO_2 + 2H_2O$) during isothermal SCR tests were calculated as follows:

$$\%CH_4(SCR) = 100 \times \frac{[NOx]_{reacted}}{2 \times [CH_4]_{reacted}}$$

$$\%CH_4(comb) = 100 - \%CH_4(SCR)$$

3. Results and discussion

3.1. Catalytic performances of the sulfated support and Pd-supported catalysts

The interpretation of TPSR profiles being useful to describe the functioning of the catalysts, it will be presented in the next section before to come across the effect of the different catalytic parameters on the steady-state SCR activities.

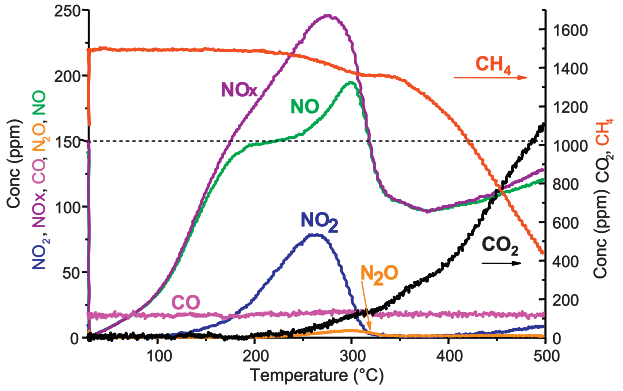

Fig. 1. Concentration profiles for NO, NO_2, NO_x, CO, N_2O, CO_2 and CH_4 measured in the course of the TPSR reaction (10 °C min^{-1}) over the Pd0.53%/SCZ28 catalyst from 25 to 500 °C under a mixture of 150 ppm NO, 1500 ppm CH_4 and 7% O_2 (GHSV = 40,000 h^{-1}).

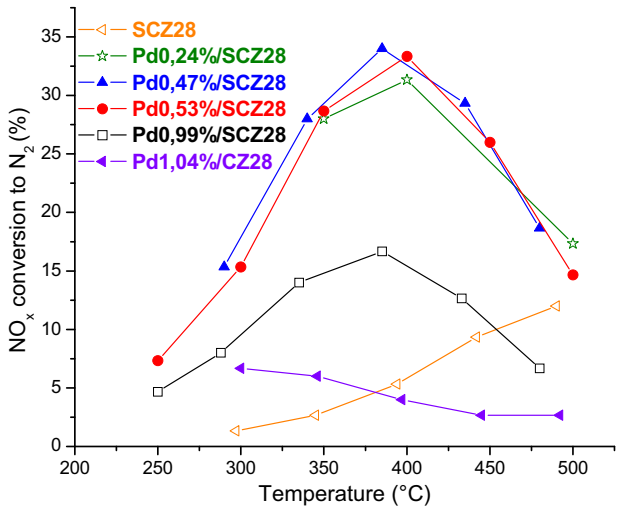

Fig. 2. Steady-state NO_x conversions to N_2 under a mixture of 150 ppm NO, 1500 ppm CH_4 and 7% O_2 (GHSV = 40,000 h^{-1}) for the different catalysts in function of the reaction temperature.

3.1.1. *TPSR patterns of supported Pd catalysts: general features*

Rather similar observations were made from the TPSR patterns obtained on the different catalysts, the latter differing only in the temperatures at which products are formed and the amounts of NO_x and CH_4 transformed or CO_x, N_2 and N_2O produced. As a representative example of an active catalyst, the TPSR profiles were reported for the sulfated 0.53%Pd/SCZ28 in Fig. 1. They are commented using a three-function $DeNO_x$ model described in [21].

The NO_2 desorption peak (max. at 263 °C) could be attributed to the decomposition of some ad-NO_x species formed via NO oxidation to NO_2 (function I, which occurs both on the support and Pd) at lower temperatures and subsequent storage of the latter on the support, namely as nitrites and nitrates [22]. Two NO desorption peaks were observed (195 °C and 300 °C). Though the former arises mainly from the redox decomposition of nitrites, yielding a nitrate species and NO [23], the second probably indicates the reaction of an ad-NO_2 species with an activated form of methane (function II occurring on Pd sites), according to the second function described in [21]:

$$NO_2 + \text{methane} \rightarrow RNO_x \rightarrow NO + C_xH_yO_z \quad (1)$$

Above 310 °C, the drastic decrease of the total NO_x below the reference level (Fig. 1) is indicative of the transformation of NO to N_2 (35% $DeNO_x$ was obtained at 370 °C), the O left during NO dissociation being scavenged by the oxygenated hydrocarbon species derived from Eq. (1) while forming CO_2 (function III [21]). It is worth noting that Pd/SCZ catalysts were highly selective for N_2, and only traces amounts of N_2O detected at the low-temperatures side of the $DeNO_x$ window. Above 370 °C, it is evident that the non-selective oxidation of methane by O_2 becomes progressively preponderant over the SCR reaction in line with the decreased NO_x removal and the "jumps" observed in the concentrations of CO_2 and CH_4 (Fig. 1).

3.1.2. *Effect of the sulfation, the Ce promoter and the Pd loading on $DeNO_x$ activity*

The SCR performances of the different catalysts measured under steady-state conditions are reported now. Over the investigated temperatures range (25–500 °C), the non-sulfated support (CZ28) was found totally inactive whereas the sulfated support (SCZ28) manifests little activity for the formation of N_2 from 350 to 400 °C, which peaks at 500 °C (12% $DeNO_x$ in isothermal mode, Fig. 2). The methane consumption by SCZ28 remained very low (<6% at 500 °C), proving that methane activation is difficult even on sulfated supports. Indeed, the superior $DeNO_x$ performances of the SCZ28 support compared with the parent CZ28 one are due to the grafting of surface sulfates during the treatment with H_2SO_4. As shown in our recent study [20] and also later on (see Section 3.2.2), the withdrawing effect brought by surface sulfate species (with a nominal density of the order of 2–3 SO_4^{2-}/nm^2) increases the amount and strength of Lewis acid sites (*cus* Ce^{x+} and Zr^{x+} cations) and creates some Brönsted acidity in the CZ material. Though the induced electronic/chemical effects may be important regarding the SCR mechanism and activity, another effects induced by sulfation are: (i) the modification of the apparent OSC (by limiting the O mobility in the CZ material); (ii) but also the NO_x/methane sorption properties. Considering the latter effect and providing that the reaction of CH_4 with NO_x follows a Langmuir–Hinshelwood mechanism [24], the reaction rate between the activated forms of methane and NO_x should be maximal at equal surface coverages. As it is common for most metal oxide surfaces, methane does not simply adsorb on the CZ and SCZ materials in its molecular form at low-medium temperatures. Rather, it is dissociated into CH_3 and H by a thermally activated mechanism, this process being often considered as the rate-determining step on the way of methane oxidation to CO_x [25]. On the other hand, the oxidation of NO by O_2 occurs readily from room temperature on CZ surfaces and induces the sorption of the formed NO_2 as nitrites ad-species, which are subsequently transformed to nitrates, the latter reaction being promoted by NO_2, O_2 and the temperature [26]. Hence, the adsorption competition is clearly at the advantage of NO_x at low-medium temperatures (as also outlined by TPSR data). On non-sulfated CZ surfaces, we have shown that these nitrates have a relatively high site occupancy of the order of 3 NO_3^-/nm^2 up to temperatures of 350 °C and above (desorption ends at 500–550 °C) [26]. By contrast, the NO_x surface coverage and the maximal desorption temperature (400 °C) of the most stable forms of nitrates is lower for the sulfated materials due to some site blockage and/or electronic effects brought by the sulfates. Hence, it could be proposed that methane activation becomes promoted only when nitrates become partially desorbed and this may contribute to explain the superior performances of the sulfated materials. Indeed, it is worth noting that the lower limit of the $DeNO_x$ temperature range on TPSR curves (Fig. 1) corresponds both to NO_2 desorption and to the onset of methane oxidation to CO_x.

The effect of sulfation on the SCR activity of Pd-supported catalysts with equal Pd loadings (about 1 wt.%) is considered now. The non-sulfated supported catalyst (1%Pd/CZ28) is only very little active in SCR with a maximum of 6% $DeNO_x$ around 300 °C in isothermal mode (Fig. 2) and 4% in TPSR mode at 320 °C (not shown

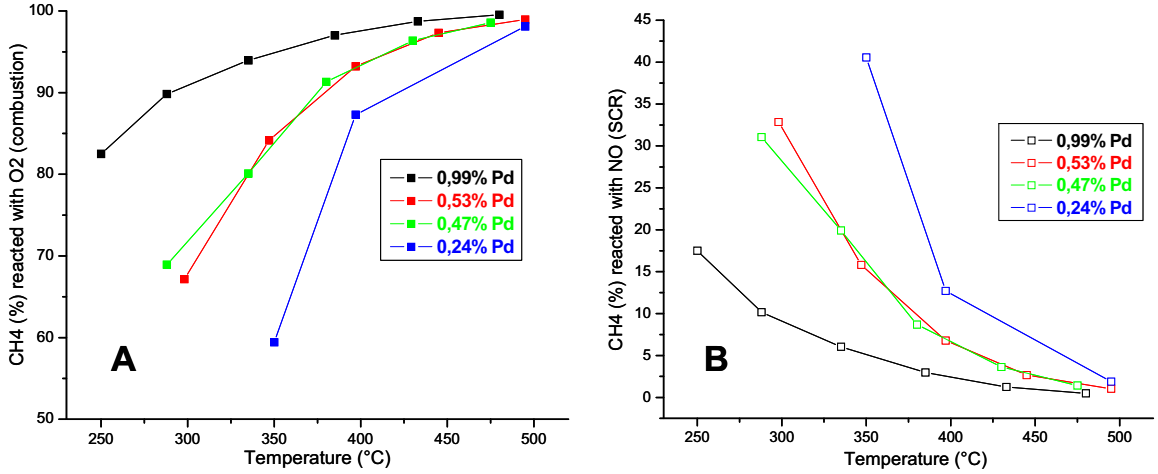

Fig. 3. Relative amounts of CH_4 used for the combustion (A) and the SCR (B) reactions during isothermal CH_4-SCR tests in function of the reaction temperature.

here). By contrast, the sulfated supported catalyst (1%Pd/SCZ28) exhibits a broader $DeNO_x$ window (250–500 °C) with a maximum of 17% N_2 at 370 °C (Fig. 2). Our results clearly confirm that the combination of sulfation with Pd is needed to enhance the SCR performances. As expected in the case of SCR catalysts, a typical "volcano" shape is obtained because the non-selective oxidation of methane by O_2 becomes progressively preponderant over the SCR reaction in the high-temperatures range. The weak performances of 1.04%Pd/CZ28 in CH_4-SCR are therefore also in line with trends reported in the literature concerning the high activity of Pd/ceria–zirconia catalysts for methane combustion [15] and the poor behaviour of reducible supports in SCR reactions [1,17].

The influence of the Pd content of the SCZ catalysts is shown in Figs. 2 and 3. By decreasing the Pd loading from 0.99 wt.% to 0.24–0.53 wt.%, a strong promoting effect is observed on the SCR performances, with 30–35% conversion of NO to N_2 in the 350–440 °C range (Fig. 2). The $T_{50}(CH_4)$ values, reflecting the methane oxidation activity of the different Pd/SCZ catalysts in the presence of NO_x, increase monotonically with the Pd content from 425 °C (0.99 wt.%) to 455 °C (0.53 and 0.47 wt.%) and 510 °C (0.24 wt.%). This indicates different uses of the hydrocarbon by the catalysts (which are better illustrated in Fig. 3A and B), and thus, the existence of different types of Pd species according to the Pd content. As described in the introduction, these trends also observed on Pd catalysts supported on acidic zeolithes and sulfated or tungstated zirconia have been rationalized by the progressive transition from Pd^{x+} isolated cations (rather active in SCR) to PdO/PdO_x clusters (rather active in methane combustion) when the Pd loading increases.

By comparing our Pd/SCZ28 samples with the literature Pd/sulfated zirconia catalysts [10], it is found that the $DeNO_x$ temperature window is shifted to the lower temperatures (by about 100 °C) in the presence of the Ce promoter. We also observed this positive effect when acidic ceria–zirconia catalysts with increasing Ce content were used for the SCR of NO_x by ethanol [27]. According to the well-known redox properties of Ce-based catalysts, one obvious effect of cerium is that Ce^{x+} sites increase both the oxidation of NO to NO_2 and the hydrocarbon oxidation activity [18]. Both reactions may be mandatory to enhance the SCR performances at low temperatures because they will help to activate the methane (see Section 3.1.1) and the lower thermostability of nitrates on Ce sites in comparison with Zr sites may also beneficial in that way [28]. At higher temperatures, the adsorption competition between NO_x (0.015%) and O_2 (7%) becomes more and more at the advantage of O_2 and the redox interplay between Pd and Ce sites (by spillover effects) may be detrimental for the SCR performances [17]. On the other hand, it is worth noting that the $DeNO_x$ activities remained almost constant in the 0.24–0.53 wt.% range for our Pd/SCZ catalysts (Fig. 2) whereas they reached a maximum for Pd/SZ catalysts at 0.1 wt.% and decreased slowly at higher loadings. It is clear that the optimal Pd loading is both function of the specific surface area of the support, the sulfate content and the nature of the Pd precursor. However, it is difficult to know if the presence of Ce also played a role in stabilizing the palladium ionic species up to higher metal loadings or even change their electronic properties. More investigations are needed to elucidate that point.

3.1.3. *Effect the CH_4:NO ratio and water vapour on $DeNO_x$*

The other reaction parameters being kept constant (7% O_2, 150 ppm NO), the methane concentration was increased from 3000 ppm (corresponding to $[CH_4]/[NO] = 20$) to 9000 ppm in order to examine the influence of the $[CH_4]/[NO]$ ratio on the NO conversion to N_2 in the case of the active Pd0.53%/SCZ28 catalyst (Fig. 4A). As expected, both the $DeNO_x$ yield and the temperature window progressively increase with the reductant concentration. However, the gain (42% $DeNO_x$ at 9000 ppm CH_4) is weak and by no means proportional to the $[CH_4]/[NO]$ ratio as was the case for $Pd,Co/Al_2O_3$ catalysts [29] under the same conditions (increase from 15% to 62% $DeNO_x$ when changing the $[CH_4]/[NO]$ ratio from 10 to 40). Anticipating our characterization results, this may be due to some differences in the nature of the active Pd phase in the two catalysts, which is itself affected by the acid–base properties of the support.

The effect of adding and removing successively 1.7% H_2O from the reaction mixture were investigated according to the temperature for the Pd0.53%/SCZ28 catalyst. As displayed in Fig. 4B, the conversion of NO_x to N_2 and to a lesser extent the methane consumption are strongly affected in wet conditions, resulting in the shift of the $DeNO_x$ window to the high temperatures and a drastic decrease in the conversion of NO to N_2. After removing H_2O from the feed (Fig. 4B), the initial SCR activity is however recovered, reaching similar $DeNO_x$ levels than before (about 30% N_2). Hence, this reversibility is indicative of some inhibiting effects on adsorption (more visible on TPSR curves), which take place namely at low-medium temperatures and become less and less significant at high-temperatures. Indeed, the presence of Ce (which lowers the $DeNO_x$ temperature) and sulfates (which probably increase the water affinity at low/medium temperatures) seem detrimental to achieve high $DeNO_x$ yields under wet conditions at medium temperatures. This could be paralleled with the better behaviour of Pd/sulfated zirconia catalysts in the presence of water around 500 °C [10].

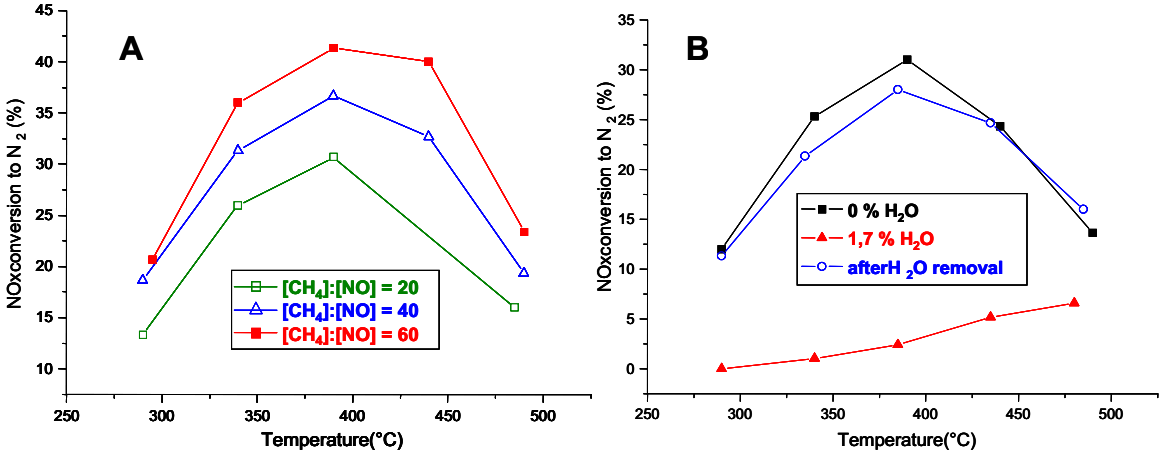

Fig. 4. Steady-state NO_x conversions to N_2 obtained over the 0.53%Pd/SCZ28 catalyst: (A) in function of the $[CH_4]$:[NO] ratio (methane concentrations were increased from 3000 to 9000 ppm, [NO] = 150 ppm, $[O_2]$ = 7%); (B) under wet (1.7% H_2O) and dry (0% H_2O) conditions in the presence of 150 ppm NO, 1500 ppm CH_4 and 7% O_2.

3.2. Characterization of the supported Pd catalysts

3.2.1. Structural characterization

As already reported [20], the preparation of sulfated CZ catalysts by direct sulfation of the crystallized oxide in sulfuric acid does not significantly alter the specific surface area and crystallite structure (Table 1) while enhancing the acidic properties. As deduced from Table 1, the presence of surface sulfates also apparently prevented the deposition of significant amounts of chlorine during the catalyst preparation, which was observed on the non-sulfated Pd catalyst. Following sulfation and deposition of palladium species with Pd loadings in the range 0.24–0.99 wt.%, no changes were detected in the XRD pattern and the Raman spectrum (not shown here) of the sulfated ceria–zirconia, which both exhibit the characteristic features of the tetragonal *t* structure of the parent mixed oxide. However, when the Pd loading was increased to 5 wt.%, a rather sharp PdO peak appeared in the XRD pattern. This indicates that for the catalysts used in the present study, Pd species are dispersed rather homogeneously on the support, at least for Pd loadings inferior or equal to 0.99 wt.%. The existence of PdO particles was neither evidenced by XRD for the non-sulfated Pd/CZ28 catalyst with 1.04 wt.% Pd.

As deduced from the examination of the sulfated SCZ28 support and some of the Pd/SCZ catalysts (0.53 and 0.99 wt.%) by HRTEM/EDX, electron micrographs were dominated by the presence of interconnected ceria–zirconia crystallites of 3–7 nm in average (Fig. 5). Though Pd was detected by EDX in most areas of the samples (inset of Fig. 5), a scrupulous analysis of related high-resolution pictures did not provide any clear evidence for the existence of supported Pd-containing particles. Therefore, this confirmed the high dispersion of Pd species, most probably as isolated cations or very small clusters (with size at least <1–2 nm) on the sulfated catalysts.

The characterization of the Pd catalysts by DR–UV–Vis spectroscopy (Fig. 6) revealed discrete changes according to the Pd loading and the sulfation treatment. It is worth noting that in the course of the calcination to 500 °C, the aspect of the Pd-loaded samples changes from yellow-pink (the colors of the ceria–zirconia powder and $PdCl_2$ precursor dissolved in NH_3) to dark yellow/orange (at low Pd loadings) or tobacco-brown (at high Pd loadings) after calcination. In DRS spectra, a weak absorption around 250 nm was only observed for the lowest Pd loadings (<0.53 wt.%) and could possibly be assigned to a $O^{2-} \rightarrow Pd^{2+}$ charge transfer band [30,31]. Taking into account HRTEM observations and the literature data, the signal detected in the region of d–d transitions, which gradually shifted from 449 to 488 nm (and increased in intensity) when the Pd loading increased from 0.24 to 0.99 wt.%, denotes the presence of small palladium entities [30–32]. The observed shift according to the Pd content has probably to be related to the transformation of isolated Pd^{n+} cations strongly interacting with the sulfated support at low Pd loadings to neighbouring Pd^{2+} in PdO_x cluster as the metal content increased to 0.99 wt.%. For

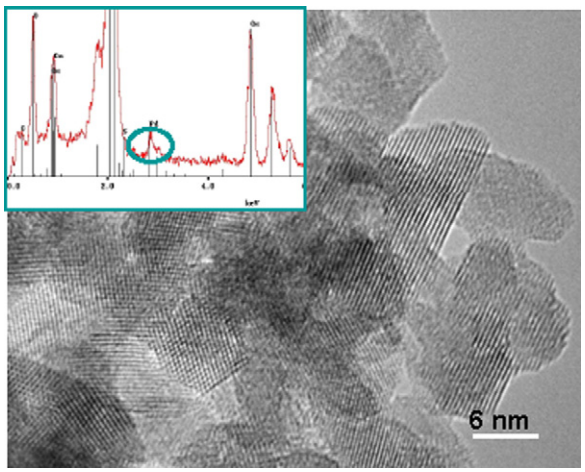

Fig. 5. Selected HRTEM image and corresponding EDX spectrum (inset) for the Pd0.99%/SCZ28 catalyst.

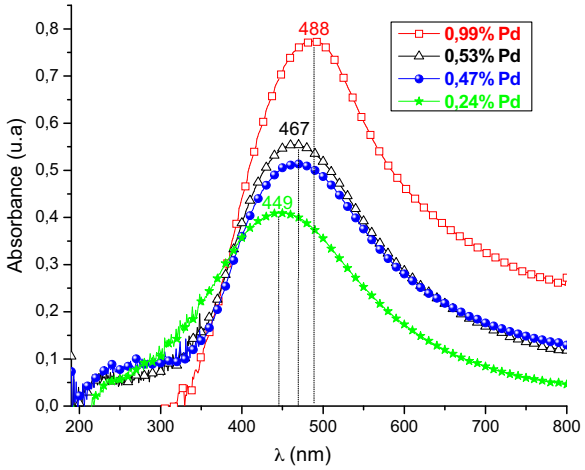

Fig. 6. UV–Vis spectra of the Pd/SCZ28 catalysts in function of the Pd loading.

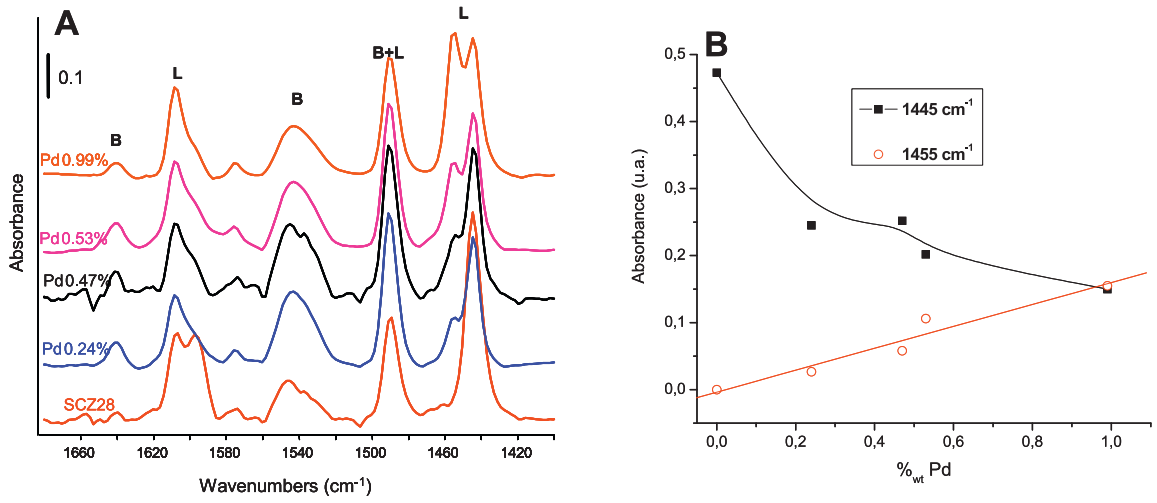

Fig. 7. (A) DRIFTS spectra of pyridine adsorbed on the different sulfated catalysts in function of the Pd loading; (B) semi-quantitative evolution of the 1445 and 1455 cm^{-1} bands in function of the Pd loading. See text for details.

the non-sulfated Pd catalyst with similar metal loading (1.04 wt.%), this absorption was shifted at 462 nm (against 488 nm for the Pd0.99%/SCZ28). This difference could be either attributed to some changes of coordination of supported Pd species on the two supports and/or to a variation in cluster size [30,31]. More information on the oxidation states and reducibility of Pd species was obtained from DRIFTS of adsorbed CO, which will be presented in a forthcoming section.

3.2.2. Acidic properties

The acid properties of the different Pd catalysts used in this study were examined by DRIFTS of adsorbed pyridine (Fig. 7A and B). The nature and strength of acid and basic sites existing on the SCZ28 and CZ28 supports have been described extensively in [20 and references therein]. The non-sulfated CZ28 support displayed only Lewis acid sites of moderate strength (*cus* Zr^{4+} and Ce^{x+} cations), as shown by the presence of absorptions at 1445 and 1608 cm^{-1}. The corresponding Pd1.04%/CZ28 catalyst exhibited the same species added to a new one located at 1453 cm^{-1} and assigned to a Py → Pd^{x+} Lewis complex. Following sulfation (Fig. 7A), the SCZ28 support displayed still one type of Lewis acid sites at the same IR frequencies that the non-sulfated one, but also Brönsted acid sites (of acidic OH type and/or bisulfate species), as revealed by the absorption at 1543 cm^{-1} (the 1489 cm^{-1} mode accounts namely for Brönsted sites but also partly for Lewis sites). In our previous study, we have demonstrated that these Brönsted sites transformed to a new type of Lewis sites (presumably more acidic) upon dehydration at moderate-high temperatures [20]. As deduced from the lack of significant variations observed for the 1543 cm^{-1} band following Pd impregnation, the amount of Brönsted acid sites did not change considerably whatever the Pd loading. By contrast, the intensity of the 1445 cm^{-1} band, ascribed previously to Lewis acid sites on the support, decreased by half whereas the one corresponding to Py → Pd^{x+} Lewis complexes (now shifted to 1455 cm^{-1}) followed a regular increase with the Pd loading (Fig. 7B). As most Pd sites were apparently accessible to the molecular probe, this led us to conclude that the dispersion of Pd species should be rather high over the range of Pd loading investigated (0.24–0.99 wt.%), therefore confirming the results obtained by HRTEM and XRD.

3.2.3. DRIFTS study of CO adsorption

By exposing the parent CZ28 support to CO at room temperature, only very weak bands were detected around 2170 and 2120 cm^{-1}, which rapidly disappeared upon evacuation under He flow. Due to the low definition of these bands, they are assigned to CO linearly adsorbed on Ce^{4+} and Zr^{4+} sites for the high-frequency band, and on reduced Ce^{3+} sites for the low-frequency one [33 and references therein]. The simultaneous detection of gaseous CO_2 in the first minutes of experiment and the build-up of weak overlapped absorptions in the 1800–1100 cm^{-1} region indicated that CO oxidation and the formation of carbonate-like species (involving basic oxygens) took also place to a little extent [17]. After sulfation, the main spectral features of the SCZ28 support above 1800 cm^{-1} were a small band at 2198 cm^{-1}, accompanied by broad shoulders centred at 2170 and 2115 cm^{-1}. In line with the literature existing on acidic zirconia and ceria catalysts [33,34], the 2198 cm^{-1} band should be reasonably assigned to M^{4+} species (M = Ce, Zr) with increased acidity due to the withdrawing electronic effect of neighbouring sulfate groups. Interaction of CO with Brönsted acid sites (as revealed by the negative absorptions in the OH region) on the SCZ material is thought to contribute also to the absorption near 2170 cm^{-1} [33]. By contrast with the parent CZ28 sample, carbonates were not observed on SCZ28. Instead, the simultaneous detection of gaseous CO_2 and adsorbed water (which induces a perturbation of some sulfate species as deduced from the negative band at 1398 cm^{-1}), is thought to involve the reaction of the CO probe with some OH groups. This confirms that the sulfated CZ has not only an acidic character (as deduced from the absence of carbonates) but also possesses oxidizing properties [20].

Because of the higher thermal stability of the resulting surface structures, IR absorptions due to CO adsorbed on Pd species at 298 K (Fig. 8) were much more intense than for the support alone at the same temperature. On the non-sulfated Pd1.04%/CZ28 catalyst (Fig. 8A), the first minutes of exposure to CO led to the build-up of intense absorptions mainly due to hydrogen carbonate (bands at 1630 and 1220 cm^{-1}), and to a lesser extent to monodentate and polydentate carbonate species (shown in Ref. [17]). The former species arises from the oxidation of CO to CO_2 on PdO clusters and the subsequent reaction of carbon dioxide with Ce^{x+}–OH^- surface groups of the support. This process was accompanied by the partial reduction of clustered palladium species, which occurred in two-steps as shown by the decrease of the band at 2145 cm^{-1} at the benefit of the 2107 cm^{-1} band and then the 2091 cm^{-1} band, in that order (Fig. 8A). These absorptions correspond to CO adsorbed linearly on Pd^{2+}, Pd^{+} and Pd^{0}, respectively [17,33]. The bands below 2050 cm^{-1} are mainly related to multi-bonded CO on Pd^0 terraces [33]. According to the literature data, absorptions at 1934 and 1882 cm^{-1} could be assigned to doubly- and triply

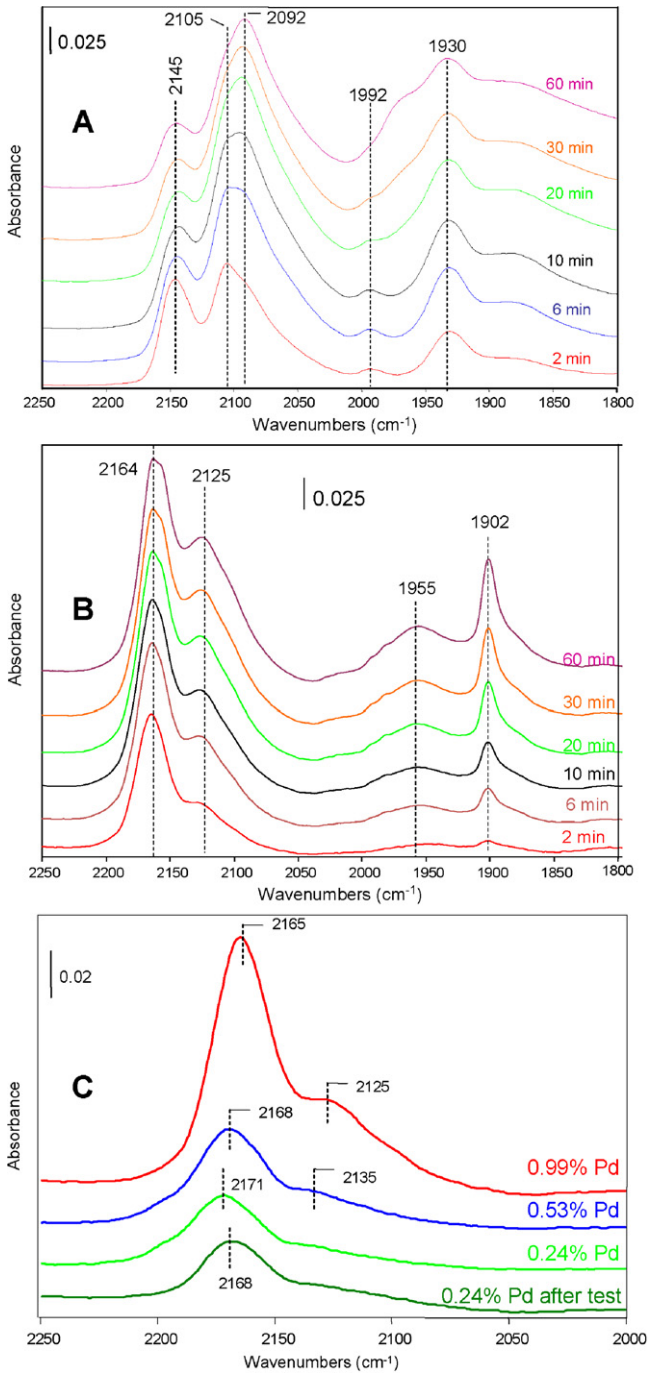

Fig. 8. *In situ* DRIFTS spectra of adsorbed CO (1000 ppm/He) at 25 °C for: (A) the non-sulfated Pd1.04%/CZ28 catalyst as function of time; (B) the sulfated Pd0.99%/SCZ28 catalyst as function of time; (C) the different sulfated catalysts in function of the Pd loading (t = 2 min).

bridged CO, respectively, on Pd(1 1 1) facets whereas the shoulder at 1970 cm^{-1} is due to adsorption on Pd(1 0 0) [33,35]. The small band at 1992 cm^{-1}, which decreases at the expense of the 1970 cm^{-1} band is due to Pd^{+}–CO–Pd^{+} species (Fig. 4A). By comparing the fraction of adsorbed CO present in linear form (2091 cm^{-1} band) to that of the bridged CO forms, it could be established that the dispersion of metallic Pd is very high [35]. By correlating these results with the absence of Pd peaks in XRD, it could be concluded that Pd species exist as very small PdO_x entities exhibiting high reducibility on the ceria–zirconia support. In a previous study [17], it was shown that these Pd species were also highly active for methane combustion.

The effect of sulfation on the state of Pd species is considered now. Due to their acidic properties, carbonate-like species were not formed on sulfated Pd catalysts [20]. Rather, weak absorptions corresponding to molecularly adsorbed CO_2 at 2355 cm^{-1} or the gas were generally observed. As expected from SCR catalytic results, the CO adsorbed species on Pd sites of the sulfated catalysts were markedly different than those described earlier on the conventional Pd1.04%/CZ28 catalyst (Fig. 8A and B). Following the first doses of CO (2 min exposure), the main bands for the Pd0.99%/SCZ28 catalyst (Fig. 4B) were located at 2164 and 2125 cm^{-1}. Upon increasing the exposure time, the latter band developed more rapidly than the former simultaneously to the growth of new absorptions at 2157, 2100, 1982, 1956, 1903 and around 1880 cm^{-1}. By comparing the time evolution of adsorbed CO species (Fig. 8A and B), it is deduced that Pd species on SCZ28 displayed less reducibility than the Pd1.04%/CZ28 catalyst into the same conditions, which points out again the role of the sulfated support in stabilizing the Pd ionic species. Moreover, the blueshift of the frequencies of linearly CO adsorbed species compared with the non-sulfated catalyst indicates an enhancement of the Lewis acidity, *i.e.* the degree of insaturation of palladium cations [33]. By decreasing the Pd loading to 0.24 wt.%, the high-frequency band observed at 2164 cm^{-1} for Pd0.99%/SCZ28 was shifted to 2172 cm^{-1} and still dominated the spectra after 100 min exposure to CO (Fig. 8C). Absorptions around 2157 and 2125 cm^{-1} very present at higher Pd loadings were also detected, but with much less relative intensity compared with the high-frequency band. The 1956 cm^{-1} band was absent and a new species, not detected for Pd0.99%/SCZ28, appeared at 1814 cm^{-1}. Upon examining the same sample after a full catalytic test in the $NO/CH_4/O_2$ reaction mixture, a similar time evolution of CO adsorbed species was noticed. Hence, no loss of dispersion or a change in the state of Pd species could be inferred following the SCR reaction. Finally, the Pd0.53%/SCZ28 catalyst displayed logically an intermediate behaviour between the two other sulfated Pd catalysts (0.24% and 0.99%). Also worth noting and as deduced from the magnitude of the signals recorded for the CO adsorbed species on the different Pd/SCZ28 catalysts, the relative dispersion of Pd species in function of the Pd loading was somewhat similar in the range investigated (0.24–0.99%), which confirms the results obtained by DRIFTS of adsorbed pyridine. In our view, this rules out the presence of large three-dimensional Pd entities on the sulfated support.

For the interpretation of DRIFTS data, we took into account some symmetric trends reported for the catalytic behaviour and the characterization of Pd catalysts supported on acidic zeolithes and sulfated zirconia in the CH_4-SCR reaction [2–10]. Hence, the evolutions observed in the state of Pd species after sulfation and in function of the Pd loading are explained as follows. On the sulfated ceria–zirconia support, the deposited Pd interact with the protons in the vicinity of Brönsted acid sites to generate either $[Pd(O)–H]^{x+}$ isolated species or small $[(PdO)_n–H]^{x+}$ clusters. These electron-deficient Pd species have both a high Lewis acidity (x should be >2) and a weak reducibility and are thought to be responsible of the high-frequency CO band observed at 2172–2164 cm^{-1} (Fig. 8C). In this concept, it seems likely that as the Pd loading increases, more Pd atoms share a proton as their amount is imposed by the sulfate content, which is constant in our case. Hence, these small Pd clusters have an inferior Lewis acidity (a lower IR frequency) as well as a superior reducibility than the isolated Pd entities (presumably more present at low Pd loadings). In the course of the exposure to CO, some $[(PdO)_n–H]^{x+}$ clusters slowly reduced giving rise to carbonyl Pd clusters such as $[Pd_n(CO)_z–H]^{y+}$ ($y < x$), which accounts for most of the absorptions observed at 2125 cm^{-1} and below 2100 cm^{-1}. In this respect, the resemblance between our IR spectra and those reported for carbonyl Pd clusters encapsulated in zeolithe supercages (with a core of 13 Pd atoms) [36]

is striking but rather intriguing taking into account that the sulfated ceria–zirconia support has no cavities. The 2157 cm^{-1} band, which also increases with the Pd loading, is assigned to some Pd cations maintaining somewhat a high oxidizing state in such type of carbonyl clusters. Taking into account the evolution of the SCR performances in function of the Pd loading, it is very probable that some "normal" PdO-like species (such as those existing on the non-sulfated Pd catalyst and active for the combustion reaction) co-exist more and more with these acidic Pd clusters as the Pd loading increases. During impregnation, these species may have been deposited on some portions of the surface which not bear sulfate groups.

4. Conclusions

In this study, the CH_4-SCR activity of Pd catalysts supported on acidic ceria–zirconia (prepared by direct sulfation of the crystallized CZ materials in H_2SO_4) was investigated according to the acidic/redox properties of the support, the Pd loading and the feed conditions.

According to the different characterizations, the Brönsted acidity of the sulfated support allowed to stabilize at the low Pd loadings highly dispersed palladium species, presumably existing as $[(PdO)_n–H]^{x+}$ adducts located in the vicinity of sulfate species. The corresponding Pd(0.24–0.53 wt.%)/SCZ catalysts displayed 30–35% NO_x conversion to N_2 around 370 °C under standard reaction conditions. By contrast, higher Pd loadings were found detrimental for the SCR activity because they also promote the formation of PdO_x clusters, which are more selective for the combustion of methane. Though the increase of the $[CH_4]/[NO]$ ratio was found to slightly promote the SCR performances, the effect of adding water to the feed was detrimental due to the inhibition of NO_x and methane sorption sites at low-medium temperatures.

Overall, the observed catalytic behaviour can be paralleled to that of Pd supported on acidic zeolithes. By comparing our results with Pd/SZ catalysts from the literature, it is deduced that cerium sites on the sulfated ceria–zirconia support acted as a promoter for the SCR reaction but also for the non-selective oxidation of methane.

Acknowledgements

The authors wish to thank the french environmental agency ADEME for its financial support throughout the Eureka project EU No. 3230 "Stationocat" (2005–2008) from which this work was part. We also greatly thank Rhodia-France for supplying ceria–zirconia samples.

References

[1] R. Burch, J.P. Breen, F.C. Meunier, Appl. Catal. B: Environ. 39 (2002) 283.
[2] Y. Li, J.N. Armor, Appl. Catal. B: Environ. 1 (1992) 31.
[3] A. Kubacka, J. Janas, E. Włoch, B. Sulikowski, Catal. Today 101 (2005) 139.
[4] M. Ogura, S. Kage, M. Hayashi, M. Matsukata, E. Kikuchi, Appl. Catal. B: Environ. 27 (2000) 213.
[5] H. Ohtsuka, T. Tabata, Appl. Catal. B: Environ. 26 (2000) 275.
[6] E. Kikuchi, M. Ogura, N. Aratani, Y. Sugiura, S. Hiromoto, K. Yogo, Catal. Today 27 (1996) 35.
[7] Z. Li, M. Flytzani-Stephanopoulos, Appl. Catal. A: Gen. 165 (1997) 15.
[8] R. Serra, M.J. Vecchietti, E. Miró, A. Boix, Catal. Today 133 (2008) 480.
[9] L. Gutierrez, M.A. Ulla, E.A. Lombardo, A. Kovács, F. Lónyi, J. Valyon, Appl. Catal. A: Gen. 292 (2005) 154.
[10] Y.-H. Chin, Walter E. Alvarez, Daniel E. Resasco, Catal. Today 62 (2000) 159.
[11] N. Li, A. Wang, X. Wang, M. Zheng, R. Cheng, T. Zhang, Appl. Catal. B: Environ. 48 (2004) 259.
[12] C.E. Quincoces, S. Guerrero, P. Araya, M.G. González, Catal. Commun. 6 (2005) 75.
[13] N. Li, A. Wang, T. Tang, X. Wang, D. Li, T. Zhang, Appl. Catal. B: Environ. 43 (2003) 195.
[14] B. Wen, Q. Sun, W.M.H. Sachtler, J. Catal. 204 (2001) 214.
[15] S. Yang, A. Maroto-Valiente, M. Benito-Gonzalez, I. Rodriguez-Ramos, A. Guerrero-Ruiz, Appl. Catal. B: Environ. 28 (2003) 223.
[16] M. Adamowska, S. Muller, P. Da Costa, A. Krzton, P. Burg, Appl. Catal. B: Environ. 74 (2007) 278.
[17] L. Zenboury, B. Azambre, J.V. Weber, Catal. Today 137 (2008) 167.
[18] A. Trovarelli, Catalysis by ceria and related materials, in: Catalytic Science Series, vol. 2, Imperial College Press, London, 2002.
[19] M. Waqif, P. Bazin, O. Saur, J.C. Lavalley, G. Blanchard, O. Touret, Appl. Catal. B: Environ. 11 (1997) 195.
[20] B. Azambre, L. Zenboury, J.V. Weber, P. Burg, Appl. Surf. Sci. 256 (2010) 4570.
[21] G. Djéga-Mariadassou, Catal. Today 90 (2004) 27.
[22] B. Azambre, L. Zenboury, F. Delacroix, J.V. Weber, Catal. Today 137 (2008) 278.
[23] B. Azambre, I. Atribak, A. Bueno-Lopez, A. Garcia-Garcia, J. Phys. Chem. C 114 (2010) 13300.
[24] I.V. Yentekakis, R.M. Lambert, M. Konsolakis, V. Kiousis, Appl. Catal. B: Environ. 18 (1998) 293.
[25] J. Wang, C. Liu, J. Mol, Catal. A: Chem. 247 (2006) 199.
[26] B. Azambre, L. Zenboury, A. Koch, J.V. Weber, J. Phys. Chem. C 113 (2009) 13287.
[27] A. Westermann, B. Azambre, Catal. Today (2010), doi:10.1016/j.cattod.2010.10.071.
[28] I. Atribak, B. Azambre, A. Bueno López, A. García-García, Appl. Catal. B: Environ. 92 (2009) 126.
[29] R. Marques, L. Mazri, S. Da Costa, F. Delacroix, G. Djéga-Mariadassou, P. Da Costa, Catal. Today 137 (2008) 179.
[30] K. Shimizu, F. Okada, Y. Nakamura, A. Satsuma, T. Hattori, J. Catal. 195 (2000) 151.
[31] Z. Boukha, M. Kacimi, M. Ziyad, A. Ensuque, F. Bozon-Verduraz, J. Mol. Catal. A: Chem. 270 (2007) 205.
[32] L.S.F. Feio, C.E. Hori, S. Damyanova, F.B. Noronha, W.H. Cassinelli, C.M.P. Marques, J.M.C. Bueno, Appl. Catal. A: Gen. 316 (2007) 107.
[33] K.I. Hadjiivanov, G.N. Vayssilov, Adv. Catal. 47 (2002) 307.
[34] C. Binet, M. Daturi, J.C. Lavalley, Catal. Today 50 (1999) 207.
[35] L. Sheu, Z. Karpinski, W.M.H. Sachtler, J. Phys. Chem. 93 (1989) 4890.
[36] L. Sheu, H. Knözinger, W.M.H. Sachtler, J. Am. Chem. Soc. 111 (1989) 8125.